ACS Photonics

pubs.acs.org/journal/apchd5

Article

Dispersion-Diversity Multicore Fiber Signal Processing

Sergi García, Mario Ureña, and Ivana Gasulla*

Cite This: *ACS Photonics* 2022, 9, 2850–2859

Read Online

ACCESS | Metrics & More | Article Recommendations | Supporting Information

ABSTRACT: Beyond playing a primary role in high-capacity communication networks, multicore optical fibers can bring many advantages to optical and microwave signal processing, as not only space but also chromatic dispersion are introduced as new degrees of freedom. The key lies in developing radically new multicore fibers where the refractive index profile of each individual core is tailored properly to provide parallel dispersion-diversity signal processing with application in a variety of scenarios such as parallel channel equalization, analogue-to-digital conversion, optical computing, pulse generation and shaping, multiparameter fiber sensing, medical imaging, optical coherence tomography, broadband measurement instrumentation, and next-generation fiber-wireless communications. Here, we experimentally prove, for the first time to our knowledge, reconfigurable two-dimensional dispersion-managed signal processing performed by a novel dispersion-diversity heterogeneous multicore fiber. The fiber comprises seven different trench-assisted cores featuring a different refractive index profile in terms of both radial geometry and core dopant concentration. As a representative application case, we demonstrate reconfigurable microwave signal filtering with increased compactness as well as performance flexibility and versatility as compared to previous technologies.

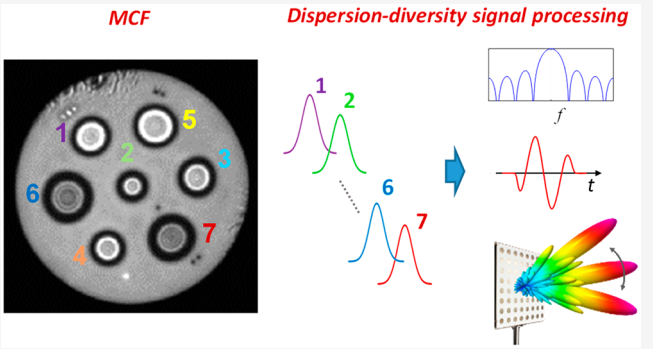

KEYWORDS: *multicore fibers, optical signal processing, space-division multiplexing, chromatic dispersion, true-time delay lines, microwave signal filtering*

INTRODUCTION

Multicore fibers (MCFs) have become one of the leading technologies to accommodate the ever-increasing capacity and parallelization demands in fiber-optic communication networks.[1] Beyond the benefits provided in terms of compactness and Shannon capacity increase, the growing interest in MCFs has recently opened up new avenues for research in emerging fields of application including, among others, data-center interconnections,[2] high-performance computing,[3] imaging, automotive lighting and control, multiparameter fiber sensing, programmable photonics,[4] quantum communications, and astrophotonics, as well as radio access networks for 5G and Beyond communications.[5]

As a new capacity to exploit, we propose here the possibility of tailoring "à la carte" the chromatic dispersion of each individual fiber core to provide parallel dispersion-managed signal processing, while the signal is being distributed. Providing the required chromatic dispersion heterogeneity, along with the exploitation of both the space and the optical wavelength dimensions, will open the way to a rich variety of 2D dispersion-managed optical signal processing applications. Figure 1 illustrates a representative portfolio of application areas that will benefit from enhanced performance regarding flexibility and versatility increase along with size, weight, and power consumption reduction. We briefly introduce below how we envision these representative applications can be enabled by the proposed dispersion-diversity heterogeneous MCFs.

Starting with optical communications networks, we find application in massive Multiple-Input Multiple-Output (MIMO) connectivity and digital signal processing by enabling both parallel chromatic dispersion compensation and group delay skew equalization simultaneously in a set of N data channels. Further digital and analogue all-optical signal processing involves recombination of a given set of temporal signal samples with different group delays, what can be easily provided after propagating through a heterogeneous MCF that acts as a sampled true-time delay line (TTDL). This finds application in optical computing including functionalities such as time differentiation (combination of positive and negative samples), time integration (combination of positive samples) or Fourier transformation (combination of suitable complex samples).[6,7] Similarly, high-speed photonic-assisted time-

Received: June 14, 2022
Published: August 4, 2022

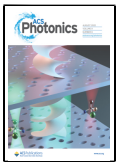

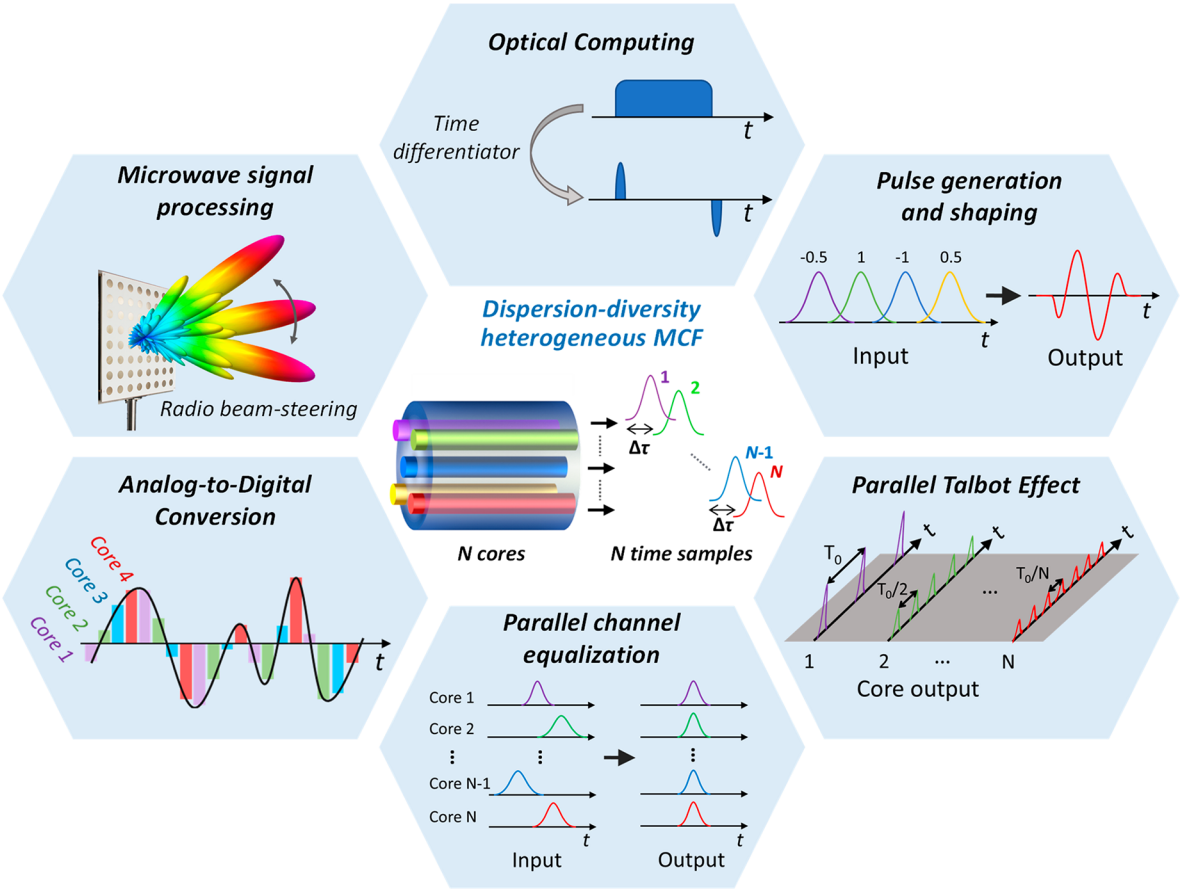

Figure 1. Representative examples of dispersion-diversity multicore fiber signal processing. The implementation of dispersion-diversity heterogeneous multicore fibers opens the door to a myriad of signal processing application fields.

interleaved analogue-to-digital converters (ADCs) can also be implemented following a similar TTDL approach.[8] In this case, the sampling rate, *fs*, of the ADC is increased by a factor given by the number of cores *N*, if the multiple time-delayed replicas of the analogue signal are sampled synchronously by electronic ADCs with sampling rates *fs*/*N* and properly recombined afterward to recover the digitized signal.

The proposed dispersion-diversity heterogeneous MCFs can offer as well different optical pulse generation and shaping techniques. For instance, we envision here, for the first time, the application of parallel temporal Talbot phenomena in MCFs to provide pulse repetition rate multiplication,[9] all-optical clock recovery,[10] or passive amplification.[11] Thanks to the Talbot effect, the temporal shape of a periodic signal that travels through a first-order dispersive medium reappears periodically at certain locations, while its repetition rate is multiplied by an integer value at some specific distance points. Therefore, since the amount of chromatic dispersion is key to implement the desired Talbot effect, we can provide parallel repetition rate multiplication if we properly tailor the dispersion of each core. Furthermore, we can implement arbitrary tunable waveform generation and shaping by combining the delayed signals coming from a given set of cores, featuring both positive and negative coefficients. Here, the appropriate differential chromatic dispersion between cores enables time-delay control by tuning the optical wavelength of the source.[12]

Another application scenario with massive impact relates to emerging fiber-wireless communication paradigms, such as Beyond 5G or 6G,[13] which demand a full integration between the optical fiber network and the wireless network while keeping the requirements in terms of high capacity, parallel connectivity, and system flexibility. Figure 2 illustrates a representative scenario where dispersion-diversity MCFs exhibit enormous potential not only to deliver parallel channels (for instance, from a central office to a set of remote multielement antennas), but also to process the microwave signal while it is being distributed to its final destination. Reconfigurable radiofrequency signal processing includes, among others, signal filtering, radio beam-steering in phased-array antennas or multicavity optoelectronic oscillation.[14]

Here, we report the design, fabrication, and experimental demonstration of the first dispersion-engineered MCF that enables 2D parallel dispersion-managed signal processing for both optical and microwave signals. The 5 km heterogeneous MCF comprises seven different trench-assisted cores, where each core features the required chromatic dispersion to provide continuous linear group delay tunability along a 30 nm optical wavelength range, while ensuring low higher-order dispersion, nonlinearity, and intercore crosstalk. As a representative application case, we have successfully demonstrated a variety of reconfigurable microwave signal filters with application in Beyond 5G communications.

RESULTS

Dispersion-Diversity Optical True-Time Delay Operation. As the core of time-discrete signal processing, an optical TTDL provides a set of time-delayed replicas of the incoming

https://doi.org/10.1021/acsphotonics.2c00910
ACS Photonics 2022, 9, 2850−2859

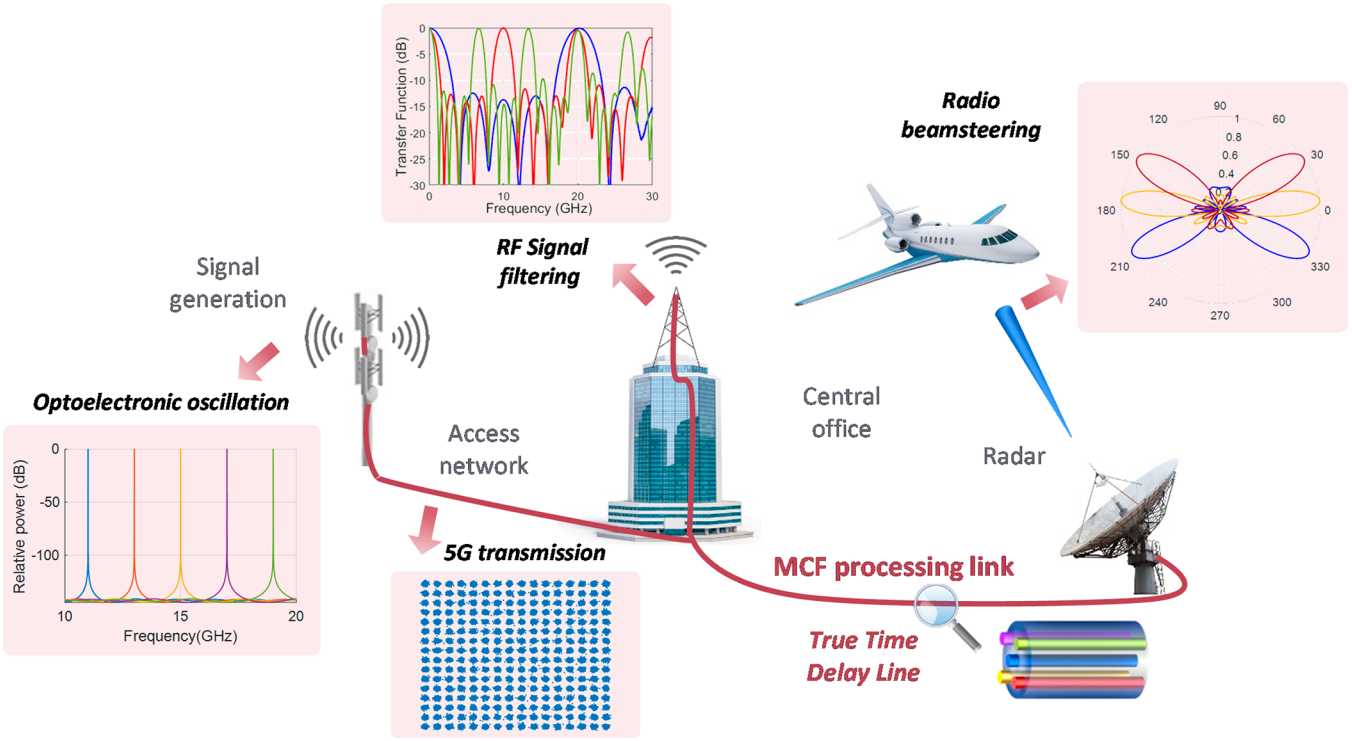

Figure 2. Application of multicore fibers to distributed microwave signal processing. Representative fiber-wireless communications scenario for Beyond 5G and 6G, where distributed dispersion-diversity signal processing leads, for instance, to radiofrequency signal filtering, radio beam-steering in phased-array antennas, and multicavity optoelectronic oscillation. Credit for some graphics used with permission: iStock.com/MR1805, iStock.com/JoeFotoIS, and iStock.com/Bet_Noire.

signal that are characterized by a constant differential delay ($\Delta\tau$; as depicted in the central inset of Figure 1). In general, we find three different approaches to induce a time delay between optical pulses: (1) variation on the group velocity along different optical wavelengths, that is, exploiting the wavelength dimension, including fiber grating inscription[15] or photonic crystal fibers;[16] (2) variation on the length between different optical fibers or waveguides, that is, exploiting the space dimension, such as switched configurations in fiber-based[17] or integrated platforms;[18] and (3) variation on the group index along different optical waveguides (fiber-based[12,19] or integrated media[20]), which can exploit both the space and the wavelength dimensions without requiring different lengths or complex configurations. The application of the last approach to provide dispersion diversity in optical fibers allows continuous time delay tunability with extended versatility and flexibility as compared to precedent solutions.

To date, we have demonstrated experimentally two sampled TTDLs based on commercial SDM fibers: (1) homogeneous 7-core MCF with inscription of selective fiber Bragg gratings[21] and (2) 4-LP-mode step-index FMF with inscription of long period gratings (LPGs).[22] However, those approaches did not provide 2D time delay continuous tunability, which requires the design of customized fibers where the chromatic dispersion of every core or mode are tailored properly. Following that principle, we theoretically proposed for the first time different dispersion-engineered SDM fibers: (1) heterogeneous 7-core doped MCF where each core features a different refractive index profile;[19] (2) 19-core photonic crystal fiber where each silica core is surrounded by a different configuration of air holes;[23] (3) 7-LP-mode ring-core FMF with an inscription of LPGs for the 4-sample operation,[24] and (4) 5-mode-group double-clad FMF for the 5-sample operation.[25] All in all, balancing both performance (in terms of crosstalk and stability) and manufacturing complexity, heterogeneous solid-core MCFs are the most promising candidate.

As presented in ref 19, the design of a heterogeneous MCF to behave as a group-index-variable delay line requires that each core features an independent group delay with a linear dependence on the optical wavelength λ. For each fiber core n, we can expand the group delay per unit length, $\tau_n(\lambda)$, in a second-order Taylor series around an anchor wavelength λ_0 as

$$\tau_n(\lambda) = \tau_0 + D_n(\lambda - \lambda_0) + \frac{1}{2}S_n(\lambda - \lambda_0)^2 \quad (1)$$

where D_n is the chromatic dispersion and S_n is the dispersion slope of core n, both at the anchor wavelength λ_0. Further development on how to model the basic differential group delay $\Delta\tau$ and the associated relative error introduced by high-order dispersion effects can be found in the Supporting Information. Figure 3a shows the spectral core groups delays in the designed 7-core fiber, where we can appreciate the basic differential group delay for a representative case in both space and wavelength diversity domains. Proper tunability requires the set of chromatic dispersions to increase constantly with the core number.

Heterogeneous Multicore Fiber Design. We designed a heterogeneous MCF for tunable TTDL operation that comprises seven distinct trench-assisted cores with a core pitch $\Lambda = 40$ μm inside a 150 μm diameter cladding. The core refractive index profiles consist of a GeO_2-doped core layer (core radius a_1 and core-to-cladding relative index difference Δ_1) surrounded by a silica inner cladding (core-to-trench distance a_2) and a 1%-fluorine-doped trench (width w), as

https://doi.org/10.1021/acsphotonics.2c00910
ACS Photonics 2022, 9, 2850−2859

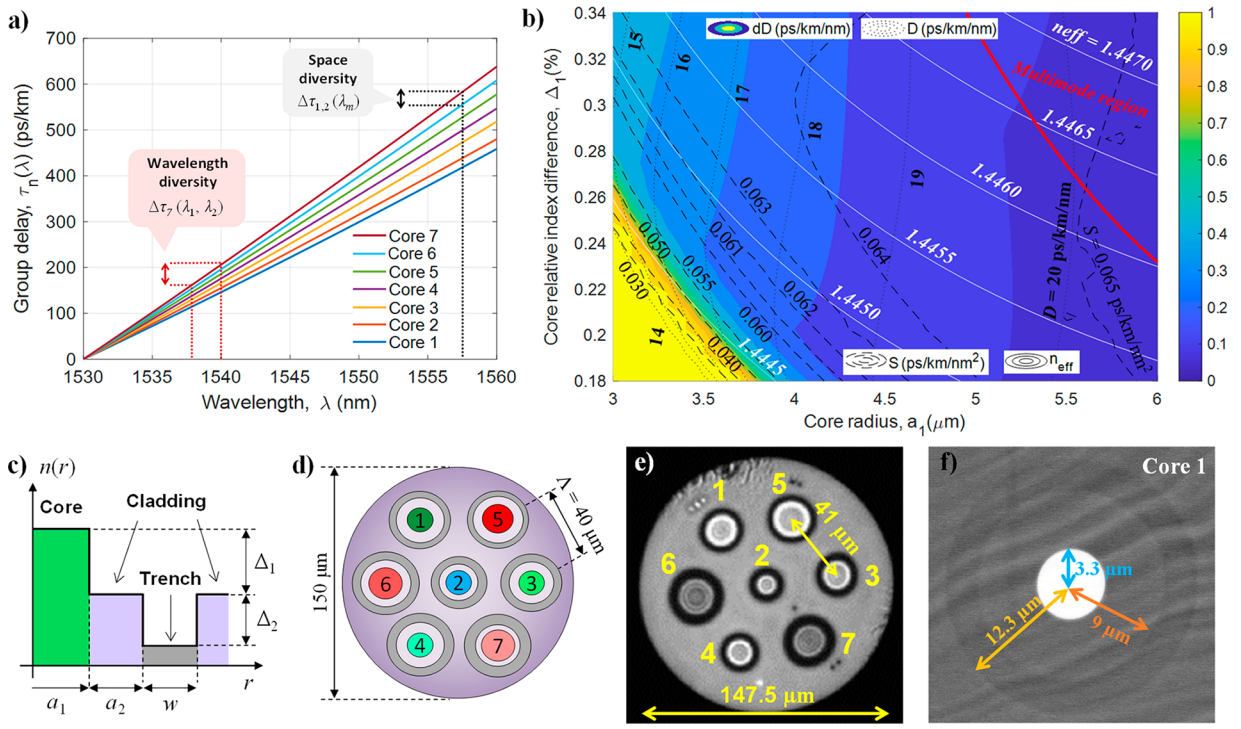

Figure 3. Design of a heterogeneous multicore fiber as a true time delay line. (a) Spectral core group delays for the designed 7-core MCF. (b) Computed chromatic dispersion variability dD (filled contours), chromatic dispersion D (dotted lines), dispersion slope S (dashed lines), and effective index n_{eff} (solid lines) as a function of the core radius a_1 (μm) and the core-to-cladding relative index difference Δ_1 (%) for $a_2 = w = 4$ μm at an optical wavelength of 1530 nm. (c) Refractive index profile of a trench-assisted core. (d) Cross-sectional area of the designed MCF where cores within the same color range comprise a group of cores with similar effective indices. (e) Cross-sectional area of the fabricated MCF. (f) SEM picture of core 1 detailing the layers' dimensions (core, inner cladding, and trench).

Table 1. Designed and Measured Core Parameters and Chromatic Dispersion at λ_0 = 1530 nm

	designed					measured				
core n	a_1 (μm)	Δ_1 (%)	a_2/a_1	w/a_1	D (ps/km/nm)	Δ_1 (%)	a_2/a_1	w/a_1	D_{CSE} (ps/km/nm)	D_{WLS} (ps/km/nm)
1	3.3	0.335	1.758	0.970	14.3	0.344	1.758	0.972	13.9	14.3
2	3.2	0.300	0.750	1.281	15.3	0.302	0.750	1.265	14.9	15.5
3	3.5	0.315	1.286	1.143	16.3	0.320	1.286	1.141	16.4	16.8
4	3.7	0.301	1.000	0.973	17.3	0.298	1.000	0.976	17.4	17.7
5	4.8	0.293	1.208	0.625	18.3	0.284	1.208	0.623	18.3	18.7
6	5.0	0.287	0.920	1.200	19.3	0.283	0.920	1.175	19.4	19.7
7	5.3	0.279	0.623	1.132	20.3	0.276	0.623	1.121	20.3	20.8

shown in Figure 3c,d. Four basic propagation parameters govern the performance of a dispersion-diversity MCF with low intercore crosstalk: group delay τ_g, effective index n_{eff}, D, and S. All cores must experience a common τ_g at an anchor wavelength with linearly incremental D and low variability between their S, while we require at least three groups of cores, each group containing a set of cores with similar n_{eff}, to ensure that each core is surrounded by cores with sufficiently different n_{eff}.[26,27] The larger the effective index difference between cores of dissimilar groups, the better the crosstalk performance.

Dispersion-diversity TTDLs are sensitive to fabrication inaccuracies that can induce chromatic dispersion mismatches. The current manufacturing tolerances are in the order of ±0.1 μm for the radial dimensions and ±0.01% for the relative refractive index differences. Figure 3b shows the chromatic dispersion variability (dD) due to fabrication tolerances (color bar) on both a_1 and Δ_1 for fixed values of the remaining design parameters. While larger a_1 provide more robustness against fabrication inaccuracies, lower a_1 are required for lower chromatic dispersions and, as less confined cores provide lower effective indices, the maximization of the range of effective indices requires at least one of the core groups to be low confined (preferably the group that contains a single core). To guarantee the maximum number of samples available after fabrication, we set the lowest-confined core to be one of the first samples (i.e., having one of the smallest D).

Using the numerical software *Fimmwave*, we tailor each refractive index profile independently by varying the core design parameters a_1, a_2, w, and Δ_1. We set a common group delay at an anchor wavelength λ_0 = 1530 nm and a range of chromatic dispersion D_n from 14.3 up to 20.3 ps/km/nm with a 1 ps/km/nm incremental dispersion at λ_0. As we see in Figure 3a, the computed spectral group delay increases linearly with the core number. The average dispersion slope variability between adjacent cores is 0.007 ps/km/nm^2, allowing a linear behavior of the space-diversity basic delay in the C+L wavelength bands. The core distribution inside the cross-sectional area of the MCF was set to minimize the intercore

https://doi.org/10.1021/acsphotonics.2c00910
ACS Photonics 2022, 9, 2850−2859

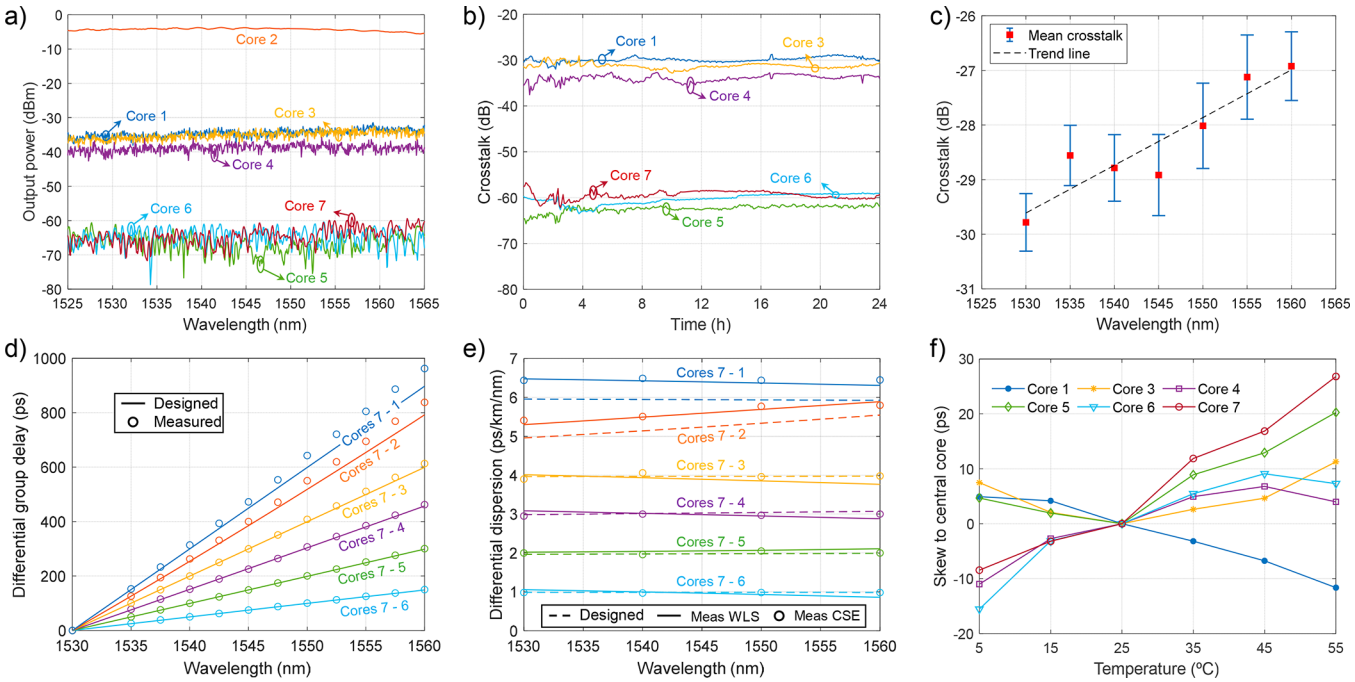

Figure 4. Experimental characterization of the true-time delay line built upon the fabricated 5 km heterogeneous MCF. (a) Measured optical output power spectra when the central core is excited; (b) Intercore crosstalk temporal evolution at 1550 nm when core 2 is excited; (c) Measured 24 h time variation worst-case crosstalk (i.e., from core 1 to core 2) for a set of representative wavelengths: markers indicate average values while bars provide the standard deviation (the dashed line acts as a visual aid to point out how the crosstalk increases on average with the optical wavelength); (d) Measured differential group delay; (e) Measured differential dispersion with respect to core 7; and (f) Temperature-dependent skew between the central (core 2) and the outer cores, normalized to the differential group delay (DGD) at 25 °C.

crosstalk, as shown in Figure 3d: group #1 is formed by core 2 (blue core); group #2 by cores 1, 3, and 4 (green cores); and group #3 by cores 5 up to 7 (red cores). The minimum effective index difference between adjacent cores is 6.8×10^{-4}, leading to a threshold bending radius of 85.5 mm, as we can see in Supporting Information, Figure S1. The core design parameters are listed in Table 1.

Heterogeneous Multicore Fiber Fabrication and Characterization. Following the design specifications, a 5.038 km MCF was fabricated by the company YOFC. The fiber is winded in a 90 mm radius spool. Figure 3e shows the cross section of the 7-core fiber, which has a cladding diameter of 147.5 μm and an average core pitch of 41 μm. Seven different preforms in terms of radial dimensions and core dopant concentration were manufactured to obtain the required propagation characteristics. Figure 3f shows the scanning electron microscope (SEM) picture of a representative core with the measured physical dimensions of its layers. Table 1 compares the designed and measured values for the layers' radial proportions and refractive index in each core, where we appreciate a considerable good match with slight variations that may be caused by fabrication tolerances and measurement inaccuracies.

Insertion Losses and Intercore Crosstalk. Characterizing the intercore crosstalk behavior depends on fiber bending and twisting,[28] optical wavelength,[29−32] modulation,[32−34] and temperature.[32] Regarding bending and twisting, we must note we have worked above the theoretical threshold bending radius of 85.5 mm, since the fiber bending radius is approximately the spool radius, that is, 90 mm.

We first characterized the intercore crosstalk in the wavelength domain. As a representative case, Figure 4a shows the measured optical spectrum of the output power when the central core (core 2) is excited. We can see how cores 1, 3, and 4 (group 1) as well as cores 5, 6, and 7 (group 2) have a similar output power level within their respective group, as they have similar effective indices. Cores from group 1 exhibit higher crosstalk than group 2, as they generally have lower mode confinement. Additionally, we observe how intercore crosstalk increases generally with the optical wavelength as the mode field diameter enlarges causing wider overlapping between adjacent cores. The output power spectra for the remaining core combinations can be found in Supporting Information, Figure S2. The insertion losses for the whole fan-in + MCF + fan-out structure range from 4.6 to 7.7 dB at 1550 nm. The optical propagation losses for each fiber core were obtained from an optical time domain reflectometer at an optical wavelength of 1550 nm as 0.46, 0.31, 0.31, 0.50, 0.19, 0.20, and 0.17 dB/km, respectively, for cores 1−7.

We measured as well crosstalk time variation in a 24 h window at room temperature. Figure 4b gathers the temporal evolution at every core output when core 2 is excited, and the central wavelength is 1550 nm. Crosstalk fluctuation relates to core position and its relationship with fiber bending and twisting along with small changes in the room temperature. The results for other representative cases (input cores 1 and 6, both at 1530 and 1550 nm) can be found in the Supporting Information, Figure S3. Figure 4c shows the worst-case intercore crosstalk, which is given between cores 1 and 2. Red squares represent the 24 h average crosstalk while error bars the standard deviation. A maximum standard deviation of 0.78 dB is obtained at 1550 nm, while the highest mean crosstalk is −26.9 dB at 1560 nm.

Experimental Evaluation of Tunable True-Time Delay Performance. We measured the DGDs for different optical wavelengths ranging from 1535 up to 1560 nm by means of an

https://doi.org/10.1021/acsphotonics.2c00910
ACS Photonics 2022, 9, 2850−2859

optical interferometric based technique (see Materials and Methods).[35] Figure 4d shows the measured DGDs between core 7 and the rest, where circle markers represent the experimental values and solid lines the designed ones. We see that the measured DGDs of cores 3 to 7 are well-matched with the designed values up to a 30 nm range, while cores 1 and 2 have been more affected by fabrication inaccuracies.

In second place, we measured the chromatic dispersion by means of two different techniques (see Materials and Methods): (1) evaluating the carrier suppression effect (CSE) that affects the RF response of the 5 km link;[36] and (2) white light source (WLS) interferometry over a short piece of fiber (39.1 cm long).[37,38] Table 1 shows the measured chromatic dispersion of each core at the anchor wavelength λ_0 = 1530 nm in comparison with the designed values. In the WLS experiment, we observe an offset dispersion of around 0.4 ps/km/nm that can be attributed to the unbalanced number of objectives between both arms of the interferometer, as discussed in Materials and Methods. Nevertheless, if we pay attention to the incremental dispersion, we can see a good agreement between the CSE and the WLS methods. Figure 4e shows the measured incremental dispersion ($D_7 - D_n$, n = 1, 2, ..., 6) as a function of the optical wavelength for the WLS (solid line) and the CSE (circle markers) experiments in comparison with our design (dashed lines). We see how the chromatic dispersion for cores 3 to 7 matches well the designed values up to a 30 nm range, while cores 1 and 2 were more affected by fabrication and do not preserve the designed chromatic dispersions. Although these two cores cannot operate as the first two TTDL samples when we exploit the fiber spatial diversity, they can however distribute two additional signal channels or implement other applications. All in all, TTDL operation by using wavelength diversity can be implemented by all seven cores.

The effect of temperature was evaluated by measuring the DGD between the central and the outer cores. The experimental setup can be found in Supporting Information, Figure S5. Figure 4f shows the average skew at different temperatures, where a maximum 35.28 ps variation is obtained for core 7. However, the temperature-controlled chamber does not only vary the temperature, but also inherently the humidity, especially for lower and higher temperatures. By taking a shorter temperature range, for instance from 15 to 35 °C, we can further reduce this humidity variation, so that the maximum skew remains below 15.08 ps (less than 1 ps/°C). As such, a small temperature variation should not cause any critical disruption in the TTDL performance. In fact, on actual deployed fiber scenarios the measured dynamic skew is in the order of picoseconds.[39] Additionally, we see that each core skew behaves differently with the temperature, which could be caused by fiber bending and twisting[40] and polarization mode dispersion.[41]

Finally, regarding bending and twisting effects on the true-time delay line performance, in[40] we studied both theoretically and experimentally how bends and twists affect the core differential group delay on a 7-core MCF. There, we showed that, although fiber curvatures can produce high group delay skew between the fiber cores (especially on the outer cores), twist-induced perturbations help to diminish this effect. Although in ref 40 we evaluated a quasi-homogeneous MCF, the effect of having heterogeneous cores is negligible as compared to the bending effect itself. On the other hand, we show in the Supporting Information that fiber bending and twisting induce a negligible effect on the core chromatic dispersions. By means of eqs 6−9 of the Supporting Information, we theoretically demonstrate that bends and twists produce a worst-case relative error below 0.1% in the core chromatic dispersions, what translates into a deviation below 2% in the differential chromatic dispersion parameter, ΔD (i.e, below 0.02 ps/km/nm).

Experimental Demonstration of 2D Distributed Microwave Signal Processing. As a representative microwave signal processing functionality, especially demanded in converged fiber-wireless communications, we experimentally demonstrate continuously tunable microwave signal filtering exploiting both the space and the wavelength diversities (i.e., 2D operation). Microwave signal filtering is implemented by combining and detecting together all the delayed signal samples coming from the MCF. The filtering frequency response depends on both the sample differential delay, which determines the filter Free Spectral Range (FSR), and the sample amplitude distribution.[14] The space-diversity differential group delay can be continuously tuned up to 150 ps by varying the optical wavelength from 1530 nm up to 1560 nm, what translates into FSRs ranging from the mm-wave band (100 GHz at 1532 nm) down to 6.7 GHz, while that for wavelength diversity varies with both the core number and the laser separation (see Figure 5a,b). Figure 5c depicts the experimental setup for the measurement of the RF filtering responses, whose description can be found in Materials and Methods.

In the space-diversity domain, our approach offers up to 5-sample operation by using cores 3 to 7, since cores 1 and 2 do not fully satisfy the TTDL condition in this regime. Figure 5d shows the measured RF filter transfer function up to 30 GHz, where blue dotted, orange dashed, yellow solid, purple dash-dotted, and green solid lines correspond to the measured responses at the operation wavelengths of 1540, 1545, 1550, 1555, and 1560 nm, respectively. We see that varying the operation wavelength continuously tunes the FSR from 20 GHz at 1540 nm down to 6.7 GHz at 1560 nm with no significant degradation. The main-to-secondary lobe level remains below −12 dB for the first filter resonances, while in the case of large operation wavelengths it increases up to −8 dB for the highest resonances.

All seven cores can be exploited in the wavelength-diversity domain, where the number of samples are given by the number of optical sources. We use an array of four lasers operating at optical wavelengths ranging from 1540 up to 1543 nm to implement a different filter in each core. Figure 5e shows the measured transfer functions of the four-tap filters created in cores 1 (blue solid line), 2 (orange dashed line), and 7 (yellow dash-dotted line) for a wavelength separation $\delta\lambda$ of 1 nm. In this case, the FSR depends inversely on the chromatic dispersion, decreasing from 14 GHz for core 1 down to 9.6 GHz for core 7. For each core, the FSR reconfigurability is given by the wavelength separation between the optical sources. Figure 5f shows the measured RF transfer functions of the same filters when the separation between lasers increases to 2 nm for wavelengths ranging from 1540 up to 1546 nm. We see how the increment on the wavelength separation reduces the FSR down to 7, 6.6, and 4.8 GHz, respectively for cores 1, 2, and 7. In all cases, the secondary lobes are kept below −10 dB even for the highest filter resonances. Reconfigurable performance of the remaining filters (cores 3−6) is demonstrated in Supporting Information, Figure S6.

https://doi.org/10.1021/acsphotonics.2c00910
ACS Photonics 2022, 9, 2850−2859

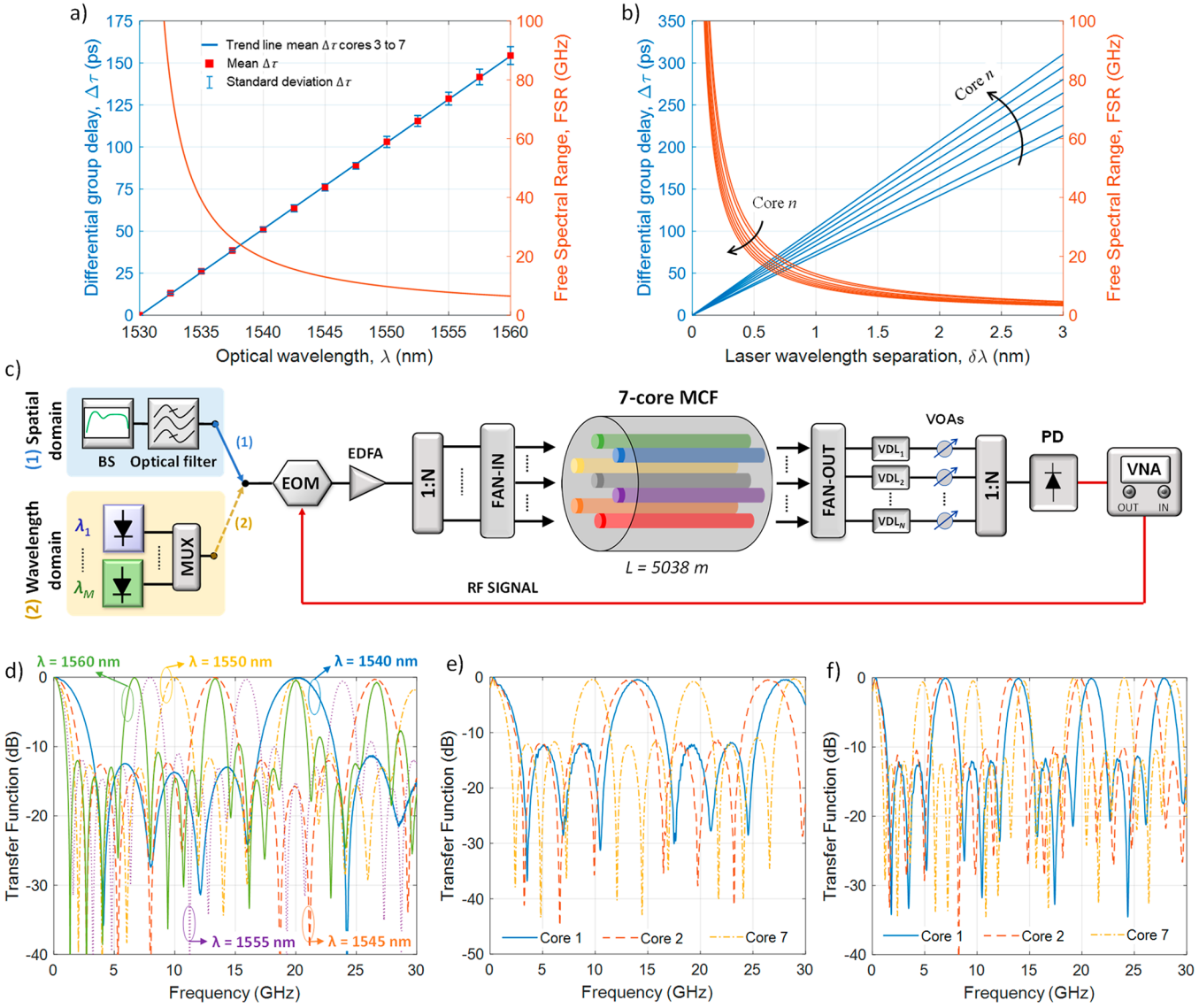

Figure 5. Experimental realization of tunable microwave signal filtering. Measured TTDL differential group delay (blue) and its associated RF processing frequency (orange) as a function of (a) the optical wavelength for cores 3−7 and (b) the laser wavelength separation for cores 1−7, respectively, for the space- and wavelength-diversity regimes. (c) Experimental setup for (1) space- and (2) wavelength-diversity domains; Measured RF transfer function for (d) the five-tap filter built upon the fabricated fiber when we operate in the space-diversity domain and (e, f) the four-tap filter built upon cores 1, 2, and 7 when we operate in the wavelength-diversity domain using a four-laser array with (e) 1 and (f) 2 nm wavelength separation between lasers. BS: broadband source, MUX: wavelength multiplexer, EOM: electro-optic modulator, EDFA: erbium-doped fiber amplifier, VDL: variable delay line, VOA: variable optical attenuator, PD: photodetector, VNA: vector network analyzer.

CONCLUSIONS

We have proposed the exploitation of dispersion-diversity MCFs to provide parallel optical and microwave signal processing while the signal is being distributed with increased compactness as well as performance versatility and flexibility. The combination of the chromatic dispersion diversity with the space and optical wavelength degrees of freedom in a single fiber will enable a comprehensive range of digital and analogue signal processing applications, going from interference-controlled signal distribution, parallel chromatic dispersion compensation, time differentiation and integration, Fourier transformation, multigigabit-per-second analogue-to-digital conversion, self-imaging phenomena (Talbot effects), optical beamforming for phased-array antennas, microwave signal filters, and instantaneous radiofrequency measurement to multicavity optoelectronic oscillation, among others. The applicability of the envisioned functionalities covers a myriad of information technology scenarios, such as broadband wireless and satellite communications, distributed antenna systems, physical, chemical, and smart structure sensing, high-performance computing, medical imaging, optical coherence tomography, broadband electronic and RF measurement instrumentation, and quantum communications.

Following this rationale, we have developed and successfully demonstrated, for the first time to our knowledge, an entirely heterogeneous MCF that provides the so-called parallel dispersion-diversity signal processing while the signal (or signals) is (are) being distributed along the fiber link. This unique capability is accomplished thanks to a novel MCF structure where each core has been drawn from a distinct preform, featuring a different refractive index profile in terms of both radial geometry and core dopant concentration.

https://doi.org/10.1021/acsphotonics.2c00910
ACS Photonics 2022, 9, 2850−2859

MATERIALS AND METHODS

Optical Losses and Intercore Crosstalk Characterization. The intercore crosstalk and the optical losses were measured by injecting the optical signal coming from a tunable laser source ANDO AQ4321D (1520−1620 nm optical wavelength range) into one of the MCF cores and measuring the outer power of all the cores via a YOKOGAWA AQ6370C Optical Spectrum Analyzer.

Differential Group Delay Characterization. The core differential group delays were measured by implementing an optical interferometer, where core 1 was used as the reference arm and the remaining cores interfered one by one. The optical signal was generated by a Yenista TUNICS T100R tunable laser source (1490−1650 nm optical wavelength range). We swept the optical wavelength of the source in a 1 nm range around the desired optical wavelengths (up to 2 nm range for optical wavelengths near the anchor wavelength λ_0 = 1530 nm, where the differential delay is smaller) to measure the interference pattern by means of a YOKOGAWA AQ6370C optical spectrum analyzer. The differential delay between cores was then obtained by calculating the Fourier transform of the measured interference pattern.

Chromatic Dispersion Characterization. The measurement of the chromatic dispersion of the fiber cores was carried out by two different techniques. For the WLS interferometry experiment, we created an interferometer between one core of the MCF and an air path (see Figure S4a of the Supporting Information). The air path is composed of four mirrors, a translation stage, two beam splitters (common to both paths), and two microscope objectives (common to both paths), while the fiber path has one mirror, the mentioned common components, and two extra objectives. We use Olympus Plan Achromat Objectives with 10× and 40× magnification and numerical aperture of 0.25 and 0.65, respectively, for the common objectives and the objectives to go throw/come from the core under test. Although the unbalanced number of objectives between both arms, which are dispersive elements, causes imbalance in the chromatic dispersion measurement, it should be noted that it is a common mismatch to all cores for each optical wavelength, so it can be treated as an offset and can be simply avoided by differentiation between cores. We used a Fyla supercontinuum laser SCT1000 as the broadband optical source, which emits more than 1 W optical power in the wavelength range from 450 up to 2400 nm, and a YOKOGAWA AQ6370D Optical Spectrum Analyzer to measure the interference pattern, which has a measurement optical wavelength range from 600 up to 1700 nm. To avoid an excessive noisy signal from the supercontinuum laser source near the pump wavelength (∼1064 nm), we selected a 400 nm bandwidth band ranging from 1250 up to 1650 nm (upper limit due to the OSA measurement range). The chromatic dispersion was calculated by fitting the phase extracted from the interference pattern with a five-element Cauchy dispersion formula.[37,38]

For the CSE experiment, we measured the RF frequency response of each core up to a 50 GHz RF frequency. We used a Yenista TUNICS T100R tunable laser source, a Photline MX-LN-40 30 GHz bandwidth Electro-optical modulator, a FINISAR XPDV3120 70-GHz bandwidth photodetector and an Agilent N4373C Vector Network Analyzer (PNA-X).

Demonstration of Microwave Signal Filtering. For the MWP filtering experiments, depending on the diversity domain exploited, we used different equipment to generate the optical signal. For the spatial diversity domain, we used a NP Photonics ASE-CL-20-S broadband source (output spectrum from 1525 up to 1610 nm wavelength range with an output optical power of 20 dBm) and an Alnair Laboratories BVF-300CL bandwidth-variable tunable optical filter (bandwidth tunability: 0.03−3 nm; center wavelength tunability: 1525−1610 nm). SSB modulation was implemented by using an ET Industries Q640−90 90° hybrid coupler that operates in RF frequencies up to 40 GHz to avoid the CSE.[36] The broadband source was used to avoid optical coherent interference, while the optical filter was required to suppress high-frequency fading effects due to the broadband source.[42] For the wavelength diversity domain, we used an EXFO IQS-2403BLD-XX-P7-EA wavelength-division multiplexing laser source providing a four-laser array with 1 and 2 nm wavelength separation in the C-band. In both cases, we used a Sumitomo T.DEH1.5-40-ADC-001 30-GHz bandwidth electro-optical modulator to modulate the RF signal coming from an Agilent N4373C Vector Network Analyzer (PNA-X). An Amonics AEDFA-23-B-FA C-band Erbium Doped Fiber Amplifier is used then to amplify the modulated signal. The signals are then treated differently depending on the operation regime. In the spatial diversity domain, the signal is split and injected into cores 3−7. After a 5 km propagation, a set of VOAs finely equalize the output power of the samples for uniform amplitude distribution before all optical signals are combined and detected together. In the wavelength diversity domain, the optical signal is injected (and photodetected) into (from) a unique core, so that every single core provides a different RF filtering functionality. In both schemes, the signals are photodetected by using FINISAR XPDV3120 70 GHz bandwidth photodetectors. Variable delay lines (VDLs) compensate minor group delay fabrication mismatches at the anchor wavelength. The electrical transfer function is measured by a PNA-X (capability up to 50 GHz RF frequencies).

ASSOCIATED CONTENT

Supporting Information

The Supporting Information is available free of charge at https://pubs.acs.org/doi/10.1021/acsphotonics.2c00910.

> Optical true-time delay model; Design crosstalk sensitivity against fiber curvatures; Insertion losses and intercore crosstalk characterization for all fabricated fiber cores; Chromatic dispersion measurement techniques; Evaluation of different degradation sources on the TTDL performance; and Additional results for microwave signal filtering in the wavelength diversity domain (PDF)

AUTHOR INFORMATION

Corresponding Author

Ivana Gasulla − *ITEAM Research Institute, Universitat Politècnica de València, Valencia 46022, Spain;* orcid.org/0000-0001-8088-7796; Email: ivgames@iteam.upv.es

Authors

Sergi García − *ITEAM Research Institute, Universitat Politècnica de València, Valencia 46022, Spain;* orcid.org/0000-0002-7237-9457

https://doi.org/10.1021/acsphotonics.2c00910
ACS Photonics 2022, 9, 2850−2859

Mario Ureña − *ITEAM Research Institute, Universitat Politècnica de València, Valencia 46022, Spain;* orcid.org/0000-0001-7283-4619

Complete contact information is available at: https://pubs.acs.org/10.1021/acsphotonics.2c00910

Funding

The authors acknowledge financial support by the European Research Council Consolidator Grant 724663, the Spanish Ministerio de Ciencia e Innovación Project PID2020-118310RB-100, and the Generalitat Valenciana Projects IDIFEDER/2018/031 and PROMETEO/2021/15, as well as the Universitat Politècnica de València PAID-10-21 fellowship for S.G.

Notes

The authors declare no competing financial interest.

REFERENCES

(1) Richardson, D. J.; Fini, J. M.; Nelson, L. E. Space-division multiplexing in optical fibres. *Nat. Photonics* **2013**, *7*, 354−362.
(2) Liu, Y.; Ma, L.; Yang, C.; Tong, W.; He, Z. Multimode and single-mode fiber compatible graded-index multicore fiber for high density optical interconnect application. *Opt. Express* **2018**, *26*, 11639−11648.
(3) Lei, F.; Dong, D.; Liao, X.; Duato, J. Bundlefly: a low-diameter topology for multicore fiber. *Proc. of the 34th ACM International Conference on Supercomputing (ICS '20)* **2020**, *20*, 1−11.
(4) Leedumrongwatthanakun, S.; et al. Programmable linear quantum networks with a multimode fiber. *Nat. Phot.* **2020**, *14*, 139−142.
(5) Special Issue on Emerging Applications of Multimode, Multicore and Specialty Fibers. *J. Sel. Top. Quantum Electron.* **2020**, *26*, na.
(6) Li, M.; Yao, J.; Azana, J.; Zhu, N. Photonic analog signal operators. *Proc. 14th International Conference on Optical Communications and Networks (ICOCN)* **2015**, 1−2.
(7) Siegman, A. E. Fiber Fourier optics. *Opt. Lett.* **2001**, *26*, 1215−1217.
(8) Xu, C.; et al. Photonic-assisted time-interleaved ADC based on optical delay line. *J. Opt.* **2016**, *18*, 015704.
(9) Azana, J.; Muriel, M. A. Temporal self-imaging effects: theory and application for multiplying pulse repetition rates. *IEEE J. Quantum Electron.* **2001**, *7*, 728−744.
(10) Pudo, D.; Depa, M.; Chen, L. R. Single and Multiwavelength All-Optical Clock Recovery in Single-Mode Fiber Using the Temporal Talbot Effect. *J. Lightw. Technol.* **2007**, *25*, 2898−2903.
(11) Jeon, J.; Maram, R.; van Howe, J.; Azaña, J. Programmable passive Talbot optical waveform amplifier. *Opt. Express* **2018**, *26*, 6872−6879.
(12) Gasulla, I.; Capmany, J. Microwave Photonics Applications of Multicore Fibers. *IEEE Photonics J.* **2012**, *4*, 877−888.
(13) Wikström, G.; et al. Challenges & Technologies for 6G. *6G Wireless Summit (6G SUMMIT)* **2020**, 1−5.
(14) Capmany, J.; et al. Microwave Photonic Signal Processing. *J. Lightw. Technol.* **2013**, *31*, 571−586.
(15) Hunter, D. B.; Minasian, R. A. Microwave optical filters using in-fibre Bragg grating arrays. *IEEE Microw. & Guided Wave Lett.* **1996**, *6*, 103−105.
(16) Sancho, J.; Bourderionnet, J.; Lloret, J.; Combrie, S.; Gasulla, I.; Xavier, S.; Sales, S.; Colman, P.; Lehoucq, G.; Dolfi, D.; Capmany, J.; De Rossi, A. Integrable microwave filter based on a photonic crystal delay line. *Nat. Commun.* **2012**, *3*, 1−9.
(17) Wilner, K.; van den Heuvel, A. P. Fiber-optic delay lines for microwave signal processing. *Proc. of the IEEE* **1976**, *64*, 805−807.
(18) Xie, J.; Zhou, L.; Li, Z.; Wang, J.; Chen, J. Seven-bit reconfigurable optical true time delay line based on silicon integration. *Opt. Express* **2014**, *22*, 22707−22715.
(19) Garcia, S.; Gasulla, I. Dispersion-engineered multicore fibers for distributed radiofrequency signal processing. *Opt. Express* **2016**, *24*, 20641−20654.
(20) Wang, J.; Ashrafi, R.; Adams, R.; Glesk, I.; Gasulla, I.; Capmany, J.; Chen, L. R. Subwavelength grating enabled on-chip ultra-compact optical true time delay line. *Sci. Rep.* **2016**, *6*, 30235.
(21) Gasulla, I.; Barrera, D.; Hervás, J.; Sales, S. Spatial division multiplexed microwave signal processing by selective grating inscription in homogeneous multicore fibers. *Sci. Rep.* **2017**, *7*, 41727.
(22) García, S.; et al. Sampled true time delay line operation by inscription of long period gratings in few-mode fibers. *Opt. Express* **2019**, *27*, 22787−22793.
(23) Shaheen, S.; Gris Sánchez, I.; Gasulla, I. True-time delay line based on dispersion-flattened 19-core photonic crystal fiber. *J. Lightw. Technol.* **2020**, *38*, 6237−6246.
(24) García, S.; Guillem, R.; Gasulla, I. Ring-core few-mode fiber for tunable true time delay line operation. *Opt. Express* **2019**, *27*, 31773−31782.
(25) Nazemosadat, E.; Gasulla, I. Dispersion-tailored few-mode fiber design for tunable microwave photonic signal processing. *Opt. Express* **2020**, *28*, 37015−37025.
(26) Hayashi, T.; Taru, T.; Shimakawa, O.; Sasaki, T.; Sasaoka, E. Design and fabrication of ultra-low crosstalk and low-loss multi-core fiber. *Opt. Express* **2011**, *19*, 16576−16592.
(27) Koshiba, M.; Saitoh, K.; Kokubun, Y. Heterogeneous multi-core fibers: proposal & design principle. *IEICE Electron. Express* **2009**, *6*, 98−103.
(28) Matsuo, S.; et al. Crosstalk behavior of cores in multi-core fiber under bent condition. *IEICE Electron. Express* **2011**, *8*, 385−390.
(29) Li, B.; et al. Role of wavelength dependent sensitivity in affecting the crosstalk mitigation of homogeneous multicore fiber: an analytical estimation approach. *Opt. Express* **2014**, *22*, 14127−14134.
(30) Ye, F.; et al. Wavelength-Dependence of Inter-Core Crosstalk in Homogeneous Multi-Core Fibers. *IEEE Photonics Technol. Lett.* **2016**, *28*, 27−30.
(31) Hayashi, T.; Taru, T.; Shimakawa, O.; Sasaki, T.; Sasaoka, E. Characterization of crosstalk in ultra-low-crosstalk multi-core fiber. *J. Lightw. Technol.* **2012**, *30*, 583−589.
(32) Yuan, H.; et al. Experimental Investigation of Static and Dynamic Crosstalk in Trench-Assisted Multi-Core Fiber. *Proc. 2019 Optical Fiber Communications Conference and Exhibition (OFC)* **2019**, 1−3.
(33) Luís, R. S.; et al. Time & Modulation Frequency Dependence of Crosstalk in Homogeneous Multi-Core Fibers. *J. Lightw. Technol.* **2016**, *34*, 441−447.
(34) Rademacher, G.; Luís, R. S.; Puttnam, B. J.; Awaji, Y.; Wada, N. Crosstalk dynamics in multi-core fibers. *Opt. Express* **2017**, *25*, 12020−12028.
(35) Dorrer, C.; Belabas, N.; Likforman, J. P.; Joffre, M. Spectral resolution & sampling issues in Fourier-transform spectral interferometry. *J. Opt. Soc. Am. B* **2000**, *17*, 1795−1802.
(36) Smith, G. H.; Novak, D.; Ahmed, Z. Novel technique for generation of optical SSB with carrier using a single MZM to overcome fiber chromatic dispersion. *Proc. International Topical Meeting on Microwave Photonics* **1996**, 5−8.
(37) Merritt, P.; Tatam, R. P.; Jackson, D. A. Interferometric chromatic dispersion measurements on short lengths of monomode optical fiber. *J. Lightw. Technol.* **1989**, *7*, 703−716.
(38) Hlubina, P., Kadulová, M.; Ciprian, D. Spectral interferometry-based chromatic dispersion measurement of fibre including the zero-dispersion wavelength. *J. Europ. Opt. Soc. Rap. Public.* **2012**, *7*. DOI: 10.2971/jeos.2012.12017
(39) Puttnam, B. J.; et al. Dynamic Skew Measurements in a Deployed 4-Core Fiber. *Proc. Conference on Lasers and Electro-Optics (CLEO)* **2020**, 1−2.
(40) García, S.; Ureña, M.; Gasulla, I. Bending and twisting effects on multicore fiber differential group delay. *Opt. Express* **2019**, *27*, 31290−31298.

(41) Azendorf, F.; et al. Group Delay Measurements of Multicore Fibers with Correlation Optical Time Domain Reflectometry. *Proc. 22nd International Conference on Transparent Optical Networks (ICTON)* **2020**, 1−4.
(42) Grassi, F.; Mora, J.; Ortega, B.; Capmany, J. Subcarrier multiplexing tolerant dispersion transmission system employing optical broadband sources. *Opt. Express* **2009**, *17*, 4740−4751.

https://doi.org/10.1021/acsphotonics.2c00910
ACS Photonics 2022, 9, 2850−2859